Chemical Engineering Journal 453 (2023) 139813

Contents lists available at ScienceDirect

Chemical Engineering Journal

journal homepage: www.elsevier.com/locate/cej

Sunflower oil as renewable biomass source to develop highly effective oil-soluble catalysts for in-situ combustion of heavy oil

Arash Tajik [a], Abdolreza Farhadian [a,b,*], Mohammed A. Khelkhal [c,*], Morteza Rezaeisadat [d], Sergey M. Petrov [e], Alexey A. Eskin [c], Alexey V. Vakhin [c,*], Meisam Babapour Golafshani [a,b], Semen E. Lapuk [c], Alexey E. Buzurov [c], Airat Kiiamov [f], Jorge Ancheyta [g,*]

[a] Department of Petroleum Engineering, Kazan Federal University, Kremlevskaya Str. 18, 420008 Kazan, Russian Federation
[b] Department of Polymer & Materials Chemistry, Faculty of Chemistry and Petroleum Science, Shahid Beheshti University, GC, 1983969411 Tehran, Iran
[c] Institute of Geology and Oil & Gas Technologies, Kazan Federal University, Kazan 420008, Russia
[d] Department of Chemistry, University of Isfahan, 81746-73441 Isfahan, Iran
[e] Kazan National Research Technological University, Institute of Petroleum, Chemistry and Nanotechnology, 68 Karl Marx St., Kazan, Russia
[f] Kazan Federal University, Institute of Physics, Kremlevskaya Str. 18, 420008 Kazan, Russian Federation
[g] Instituto Mexicano del Petróleo, Eje Central Lázaro Cárdenas Norte 152, San Bartolo Atepehuacan, Mexico City 07730, Mexico

ARTICLE INFO

Keywords:
Environmental effects
In situ-combustion
Aquathermolysis
Oil-soluble catalyst
Heavy oil
Sunflower oil

ABSTRACT

In-situ combustion has received much attention in the last few decades for enhanced heavy oil recovery processes. Although a wide part of research efforts has only focused on the application of different oil soluble catalysts to improve the combustion flame stabilization, the effect of ligand structure and metal–ligand interactions on the performance of heavy oil oxidation in presence of oil soluble catalysts is poorly understood. In this study, sunflower oil as an eco-friendly and cheap source was used to synthesize a new ligand for the preparation of Fe, Ni, Co and Cu-based oil soluble catalysts. The interaction of metals with the ligand was investigated by computational study and the results revealed that Cu-based catalyst was the most effective catalytic system for enhancing heavy oil oxidation process because it possessed the strongest bond energy with the ligand at different temperatures. Subsequently, the impact of oil soluble catalysts on the oxidation of heavy oil was investigated via non-isothermal kinetics and thermodynamic studies using thermogravimetric (TG/DTG) and differential scanning calorimetric analyses (DSC) combined with the isoconversional (Friedman and Kissinger-Akahira-Sunose), and model-based approaches. As anticipated, the kinetic and thermodynamic data demonstrated the efficiency of the used catalysts on the process of heavy oil oxidation process and proved a maximum temperature shift of ~ 120 °C in high-temperature oxidation zone. To the best of our knowledge, this is the first superior catalyst among investigated oil-soluble catalysts for heavy oil oxidation. The evidence from the obtained results points toward the idea that the choice of the ligand and the associated metal is crucial to achieve the highly active and smart catalytic system for enhanced oil recovery methods.

1. Introduction

The worldwide energy demand and consumption has increased dramatically in recent years due to the rapid growth of population and various industries. Since the amount of unconventional oil resources such as heavy and extra-heavy crude oils is much higher than conventional oil reserves (light crude oil), they can well meet the energy needs of the world in the future [1]. However, unconventional oil resources are difficult to extract and transport because of their intrinsic properties such as low API gravity, high viscosity, poor fluidity, and more complex structure than conventional oil, which originates from the presence of higher amounts and structure of asphaltenes and resins fractions [2,3]. Therefore, the oil industry has significantly invested in developing extraction methods and improving the heavy oil transportation process based on the reduction of the oil viscosity [4]. In the last two decades enhanced oil recovery (EOR) methods have attracted significant

* Corresponding authors at: Department of Petroleum Engineering, Kazan Federal University, Kremlevskaya Str. 18, 420008 Kazan, Russian Federation (A. Farhadian).
E-mail addresses: AFarhadian@kpfu.ru (A. Farhadian), MHelhal@kpfu.ru (M.A. Khelkhal), Vahin-a_v@mail.ru (A.V. Vakhin), jancheyt@imp.mx (J. Ancheyta).

https://doi.org/10.1016/j.cej.2022.139813
Received 16 August 2022; Received in revised form 10 October 2022; Accepted 12 October 2022
Available online 17 October 2022

attention as an efficient technology to improve heavy oil production [5,6]. Among the EOR approaches, in-situ combustion (ISC), which is a subset of thermal injection is considered promising thermal EOR method to reduce heavy oil viscosity [7–12]. During ISC, a stream of air under high pressure is injected to provide the necessary conditions for oxidation reactions inside the reservoir [6,13,14]. This increases the reservoir pressure and decreases the viscosity of the crude oil, enhancing the mobility of heavy oil [15]. In general, thermal oxidation process of heavy oil can be divided into three main parts: 1) low-temperature oxidation (LTO) as the initial stage, 2) medium-temperature oxidation (MTO), causing the formation of fuel deposits (FDs), and 3) high-temperature oxidation (HTO) [16,17]. The oxidation of crude oil begins by injecting air into the reserves. After the induction period, the oil starts to ignite, which creates a combustion front, and then it moves in the direction of air injection [13,18]. The combustion front propagation is a complicated chemical and physical transport process in porous media, including heat, momentum, and mass transfer combined with complex chemical reactions [19]. ISC is a low-cost method of thermal energy delivery as the heat is generated inside the reservoir [20,21]. It is also worth to mention that the amount of sulfur in heavy oil is partially eliminated using ISC method, improving the oil quality [22,23]. Although some successful field applications of ISC have been reported [19,20], it is not widely used in oil fields due to instability of combustion front, difficulties in the ignition step and process control [20]. It has been proposed that the usage of catalysts can significantly improve the ignition rate and create a self-sustained combustion front [24]. Various catalysts based on transition metals (TM) and their oxides particles are commonly used for this purpose because they can effectively adsorb and activate oxygen or oxygen species as well as they can get involved in the propagation step where radicals are (re)generated [24–26]. Moreover, the high heat transfer coefficient of metals has a significant effect on the efficiency of thermal EOR [27,28]. For example, it has been documented that the use of iron and copper nanoparticles plays an important role in improving the combustion process, maintaining temperature in LTO, and reducing water produced in the ISC process [24,28,29]. Nevertheless, insolubility of metals and their oxides in oil causes their aggregation, which decrease the efficiency of the catalytic system. Therefore, the research has been focused on oil-soluble catalysts in recent years because they can provide higher distribution degree in crude oil [26,30,31]. Oil-soluble catalysts consisted of one or more TM and an organic ligand such as fatty acids. Thus, they form a complex in which the organic ligand dissolves the metal in the crude oil and prevents the aggregation of metal particles [26,32,33]. Carboxylate TM with the chemical formula $(\text{R-COO}^{-})^{n}\ (\text{TM})^{n+}$ is the most basic oil-soluble catalysts for thermal EOR because of its low cost and easy access to sub-acids [26,33,34]. Furthermore, they are readily prepared by ion exchanging of sodium carboxylate with metal salts or neutralizing carboxylic acids with metal hydroxides at low temperatures [35–37]. A maximum reduction of 74 % in heavy oil viscosity was observed using a catalyst composed of oleic acid and iron [38]. Suwaid et al. [39] developed copper-stearate (CS) and copper-oleic (CO) as oil-soluble catalysts for thermal EOR application. The results of saturate, aromatic, resin, and asphaltene (SARA) analysis showed that in presence of CS and CO the amount of aromatics compounds decreased from 44.32 % to 40.01 % and 38.05 %, and asphaltenes decreased from 5.91 % to 4.82 % and 3.98 %, respectively. Khelkhal et al. [40] investigated the effect of nickel talattes and cobalt talattes on the oxidation kinetics of heavy oil. They found that both catalysts decreased the activation energy in the HTO region and enhanced the reaction rate. Although, different oil-soluble catalysts based on fatty acids have been studied to enhance the reaction rate of heavy oil oxidation, the interaction of ligands with metals is poorly understood. In the present research, we introduce sunflower oil as a renewable biomass source to develop scalable ligands to design effective oil-soluble catalysts. The synthesized ligand has a more complex structure than fatty acids, providing new insight into the effect of ligand–metal interactions on heavy oil oxidation process in the oil-soluble catalysts. The ligand-metals interaction in addition to the physical properties of the obtained catalytic systems were investigated by a set of physical and chemical analysis (FT-IR, XRD, SEM) combined with computational study.

2. Experimental section

2.1. Materials

A sample of Aschalcha heavy crude oil, HCO was provided by PSJ Tatneft, Republic of Tatarstan, Russia and its physical–chemical properties are summarized in Table 1. The inorganic salts and the 43–64 μm pure quartz sand fraction were obtained from Sigma-Aldrich. Sunflower oil (SFO) was supplied from supermarket. Formic acid (FA), hydrogen peroxide (H_2O_2), dichloromethane (DCM), magnesium sulfate ($MgSO_4$), Perchloric acid (PA), and tetrahydrofuran (THF) were purchased from Sigma CO.

2.2. Synthesis of sunflower oil-based ligand (SFOL)

The epoxidation/oxirane ring-opening approach was used to prepare SFOL. Epoxidized sunflower oil (ESFO) was synthesized according to literature [41–43]. Following, 100 g of ESFO and 200 mL of THF were mixed in a 1000 mL flask, and 400 mL of 20 wt% PA was added dropwise to the flask at 25 °C. After 20 h, the aqueous solution was decanted and THF was evaporated to attain SFOL. The chemical structure of SFOL is shown in Fig. 1.

2.3. Preparation of oil-soluble catalysts (OSCs)

Metal salts ($FeCl_2{\cdot}4H_2O$, Cu (NO_3) 2·.$3H_2O$, $CoCl_2{\cdot}6H_2O$, and Ni (NO_3) 2·.$6H_2O$) and SFOL were used to prepare OSCs in a 1:3 M ratio. The ligand was first dissolved in ethanol and mixed well with a mechanical stirrer for 20 min. The pH of the ligand solution reached 9 by adding NaOH. Then, a mixture of metal salt-ethanol was added to the ligand solution dropwise and was stirred for 45 min. Finally, the resulting solids were filtered and washed three times to remove ligand and excess salt. The obtained OSC was dried at room temperature for 18 h. The synthesized OSCs represent by following abbreviations:

$$\text{Fe} + \text{ligand} \rightarrow \text{Fe-OSC},\ \text{Co} + \text{ligand} \rightarrow \text{Co-OSC}$$

$$\text{Ni} + \text{ligand} \rightarrow \text{Ni-OSC},\ \text{Cu} + \text{ligand} \rightarrow \text{Cu-OSC}$$

2.4. Sample preparation for thermal analysis

A sample of HCO was mixed with pure quartz sand fraction in a 1:9 ratio to perform the non-catalytic experiments of HCO oxidation process. Additionally, all HCO catalytic oxidation experiments were carried out using 2 wt% of OSCs.

2.5. Thermal analysis

The kinetic and thermodynamic behavior of the HCO oxidation in presence and absence of OSCs was studied by an STA 449 F1 Jupiter (Netzsch) thermoanalyzer at a temperature range of 30–600 °C with heating rates of 5, 10, 15, 20 °C min^{-1} and 50 mL min^{-1} air flow. This instrument provides simultaneous differential scanning calorimetry (DSC) and thermogravimetric (TGA) analysis data. These data were processed and interpreted by Proteus Analysis v5.2.1, NETZSCH Kinetics Neo 2.1.2.2 program package.

2.6. Kinetic analysis

To understand the relation between OSCs and the processes of heavy

Table 1
Properties of Ashalcha heavy crude oil.

Viscosity at 20 °C (mPa × s)	Density at 20 °C (g × cm^{-3})	API gravity	Elemental content (%)				SARA analysis (%)			
			C	H	N	S	saturated	aromatic	resins	asphaltenes
11 811	0.97	13.8	82.09	10.12	0.63	2.65	26.2 ± 0.5	44.1 ± 0.6	26.3 ± 0.5	4.5 ± 0.3

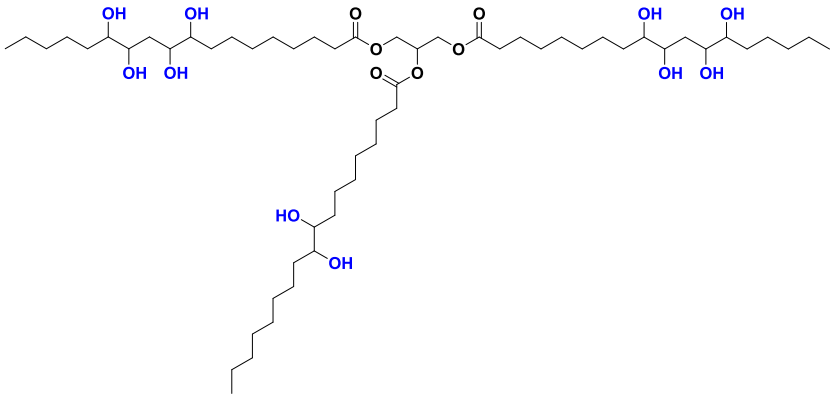

Fig. 1. Molecular structure of SFOL.

oil oxidation kinetics and its thermodynamic behavior, the isoconversional and model approaches of non-isothermal kinetics were applied [44,45] by taking into consideration the recommendations of the International Confederation for Thermal Analysis and Calorimetry (ICTAC). According to the isoconversional principle, the reaction rate of HCO oxidation process at a constant conversion can be a function of temperature only. Thereby, Friedman's analysis [46] and the Kissinger-Akahira-Sunose methods were used to calculate the thermodynamic and kinetic parameters of the HCO oxidation in presence and absence of OSCs. However, providing accurate results requires combining the calculated kinetic and thermodynamic parameters from the isoconversional methods to those obtained by model-based methods. Therefore, minimizing experimentally measured and calculated data differences on the reaction rate was used to select the appropriate model for the process of HCO oxidation [44]. The models used in this study are shown in Table 2 [47–49]. Thus, the conversion times at different conversion degrees were predicted to estimate the catalysts efficiency [50,51].

2.7. Computational method

Computational studies including molecular dynamics (MD), quantum methods (QM), and hybrid quantum mechanics/molecular mechanics (QM/MM) [52,53] are essential for predicting the electronic structure, bonding nature, and interactions of molecules. The electronic structure of SFOL was investigated with respect to properties such as partial charge distribution, electron density and molecular electrostatic potential (MEP). These properties predict which parts of SFOL most likely interact with the metals. In the next step, the interaction and formation of bonds between these points with metals (Co, Cu, Fe, and Ni) and the strength of these bonds were examined. Finally, the bond strength between the metal and SFOL was determined for the strongest bond at different temperatures. All initial structures of SFOL and the metals were drawn by Gaussview06 [54] program and fully optimized using Gaussian09 [55] software. A common method of density functional theory with hybrid exchange–correlation B3LYP functional [56] was used for all calculations. The Dunning [57] double-zeta correlation-consistent basis sets plus diffusion functions (aug-cc-pvdz) for all structures were applied. All calculations were performed in the heptane medium by implicit solvent model [58]. Some useful properties and energies related to the optimized structures were obtained. The binding Gibbs free energy (ΔG_b) of the metal- SFOL complex is defined as following equation [59]:

$$\Delta G_b = \Delta G_{Metal-SFOL} - (\Delta G_{Metal} + \Delta G_{SFOL}) \quad (1)$$

where $\Delta G_{Metal\text{-}SFOL}$, ΔG_{Metal} and ΔG_{SFOL} are the Gibbs free energy of the Metal- SFOL complex, metal, and SFOL, respectively. Gibbs free energies were obtained by frequency calculations.

Table 2
Models used for the calculation of kinetic parameters.

Model	Equation
Reaction of nth order (Fn)	$f = (1\text{-}\alpha)^n$
N-dimensional nucleation according to Avrami-Erofeev (An)	$f = n\cdot(1\text{-}\alpha)\cdot[-\ln(1\text{-}\alpha)]^{(n\text{-}1)/n}$
Expanded Prout-Tompkins equation (Bna)	$f = (1\text{-}\alpha)^{\ n}\cdot\alpha^{AutocatOrder}$
Reaction of nth order with m-Power autocatalysis by product (Cnm)	$f = (1\text{-}\alpha)^n\cdot(1 + AutocatOrder\cdot\alpha^m)$

3. Results and discussion

3.1. Characterization of OSCs

Hydroxyl groups of SFOL are the main functional group of the ligand to coordinate with different metals and form a complex. Therefore, any change in intensity or displacement in the position of hydroxyl peaks indicates the formation of a complex between the ligand and the metal. In FT-IR spectrum, a hydroxyl group can be characterized by peaks at 3100–3600 cm^{-1}, 1020–1200 cm^{-1}, and 1087–1124 cm^{-1} related to –OH, C-OH, and C—O, respectively. As can be seen in Fig. 2, a significant shift is observed in the position of hydroxyl peaks for OSCs compared with SFOL.

XRD analysis was also performed to further confirm the complex formation. Fig. 3 displays XRD pattern of the synthesized OSCs. As seen in Fig. 3, no obvious traces of the metal salts and the corresponding oxides were observed in their related patterns. These results confirm the successful synthesis of complexes between the ligand and metals.

Additionally, the morphology and the size of metals in OSCs was investigated by SEM and the corresponding images are shown in Fig. 4. It is seen that Cu nanoparticles are more spherical than Fe, Ni, and Co, providing higher contact surface with HCO and enhancing the efficiency of oxidation. Moreover, most of Fe, Ni, Co, and Cu nanoparticles in Fe-OSC, Ni-OSC, Co-OSC, and Cu-OSC have a particle size in the range of

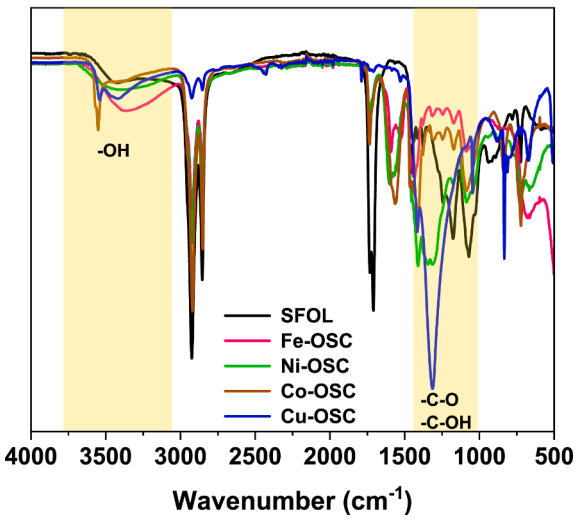

Fig. 2. FT-IR spectrum of SFOL and OSCs.

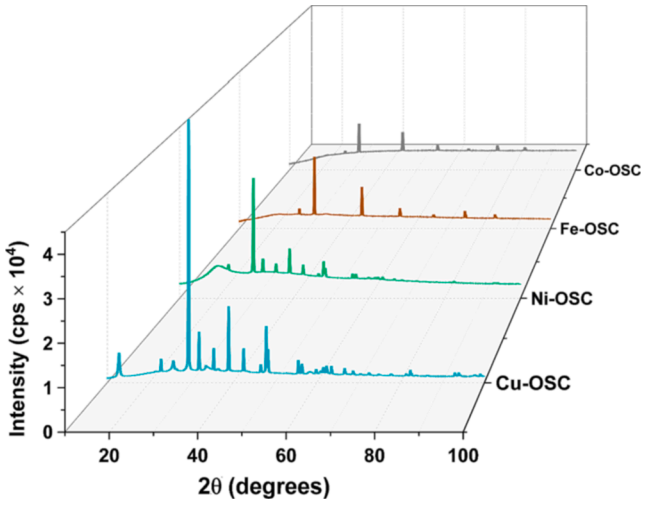

Fig. 3. XRD patterns of synthesized OSCs.

37–127 nm, 66–138 nm, 86–333 nm, and 22–70 nm, respectively.

It has been reported [33,60] that nanoparticles with a smaller size considerably increase heat transfer coefficient of the system, intensifying the random motion and collision between fluid molecules and the nanoparticles. These results suggest that Cu-OSC with smaller nanoparticles of Cu may have a greater effect on the HCO oxidation process than other nanoparticles.

3.2. Computational investigation

The interaction energy between SFOL and metals as well as the stability of SFOL-metal bonds at different temperatures were studied using computational methods to investigate the effect of ligand–metal interactions on in-situ oxidation of HCO. Generally, molecular dynamics method or alternative molecular model are used to reduce the computational costs of large molecular systems with a large number of atoms [61,62]. Since SFOL is a branched macromolecule and has several functional groups (Fig. 5a), it is difficult to predict the points that tend to interact and bind to the metals.

Due to the lack of symmetry in SFOL structure, the electronic properties vary in different parts of the molecule. One of these properties is related to the partial charge distribution on the atoms, which causes the asymmetry of the electronic density distribution. Natural bond orbital (NBO) [63] method was used to calculate partial charge distribution and the results are displayed in Fig. 5b. Additionally, the energy gap is usually considered a measure of the stability of a structure [64]. The greater energy gap indicates a more stable structure and vice versa. The gap energy shows the energy difference of highest-occupied molecular orbital (HOMO) and lowest-unoccupied molecular orbital (LUMO), which are depicted in Fig. 6. These orbitals represent the active area that are mostly involved in reactions and interactions. The value of energy gap for SFOL is 0.27 eV.

In addition, molecular electrostatic potential (MEP) energy level that depends on electron density, is another important parameter for understanding the relationship between potential energy and molecular structure as well as the positioning of structures for interactions with each other [65]. Fig. 7 shows the three regions of SFOL with different electron density. It can be predicted that the interaction of SFOL occurs between its hydroxyl groups and the metal cluster. The results of partial charge distribution, molecular orbital, and MEP predict that the most probable interaction of metals with SFOL takes place in regions a, b, and c.

In a comparative study, the bond strength between oxygen of regions a, b, and c with Fe, Co, Ni, and Cu was evaluated individually. The results of the bonding energy between oxygen in different parts of SFOL with the metals are presented in Fig. 8.

According to Fig. 8, regarding the bond strength between part a (P_a) and the metals, it is predicted that the highest value is related to P_a-Cu > P_a -Ni > P_a-Co > P_a-Fe. Moreover, the bond strength for part b (P_b) and part c (P_c) are in the following order: P_b-Cu > P_b-Ni > P_b-Fe ≈ P_b-Co and P_c-Cu > P_c -Ni > P_c-Co > P_c-Fe, respectively. It is worthwhile noting that the bond strength between Cu and different parts of SFOL is significant and it has the highest tendency to bond with SFOL. There is no significant difference in the bond tendency between P_a and P_c for all metals, but in general, P_c shows a greater bonding energy, which is probably more related to the active molecular orbital region and low electrostatic repulsion. As mentioned, three regions of SFOL can form bonds with the metals, which have a favorable energy. Therefore, there is a possibility of synergy in the bonds between SFOL and the metals. According to sum values of binding energy, this synergy occurs in all the studied metals, but with varying degrees of intensity. The synergistic effect in the formation of bonds between different parts of SFOL with the metals increases the bond strength between them in the complex. The highest synergy effect for Cu was observed for P_c as compared to P_a and P_b. Furthermore, the change in the bond strength between SFOL and different metals was investigated at high temperatures (250 °C, 350 °C, and 450 °C) using frequency calculations. The results are shown in Table 3.

Table 3 demonstrates that the bond strength between the metal and SFOL decreased as temperature increased from 25 °C to 450 °C and it is practically negligible at 450 °C. The highest and lowest reduction in the bond strength were observed for Cu and Ni, respectively. This can be the main reason for the best efficiency of Cu-OSC on oxidation process of HCO as it kept most of Cu until 250 °C and released the metal at 350 °C. This behavior results in a sudden release of 35.6 kcal/mol at 350 °C (Fig. 9), which significantly enhanced the oxidation process. However, Fe and Co more easily separated from the ligand at temperature lower than 250 °C. These results signify that if the interaction between a ligand and metal is high, their complex would break at higher temperature, resulting in a better efficiency on oxidation process of HCO. These observations confirm that the structure of ligand plays a significant role on the HCO oxidation process through its interaction with metals in OSC systems.

3.3. Thermal analysis of heavy oil oxidation in presence and absence of the obtained catalysts

To understand the behavior of HCO oxidation processes in the absence and presence of OSCs, thermal analysis was performed. It is

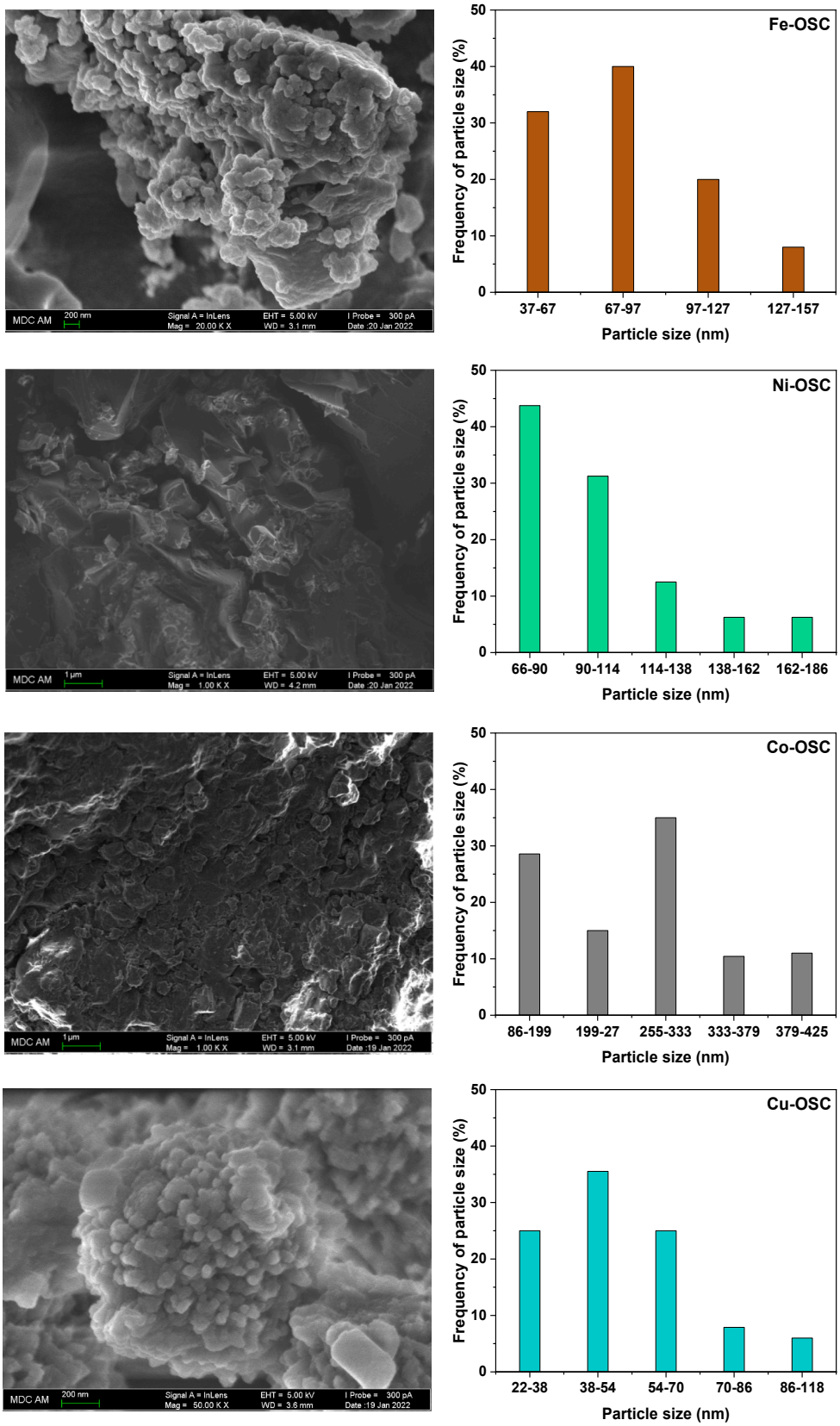

Fig. 4. SEM images and particle size frequency of OSCs.

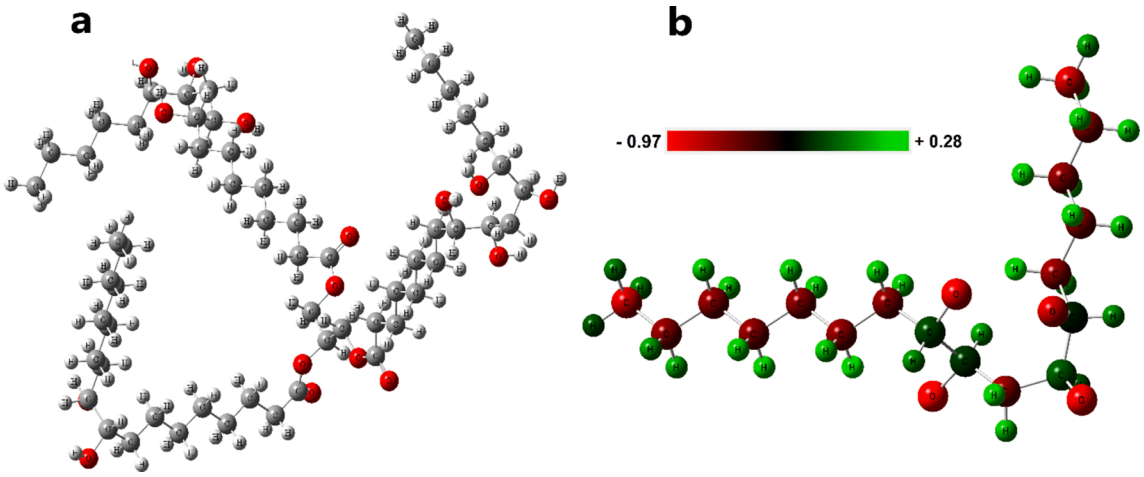

Fig. 5. Optimized structure of SFOL (a) and schematic partial charge distribution of SFOL (selected small portion of SFOL for clarity) (b).

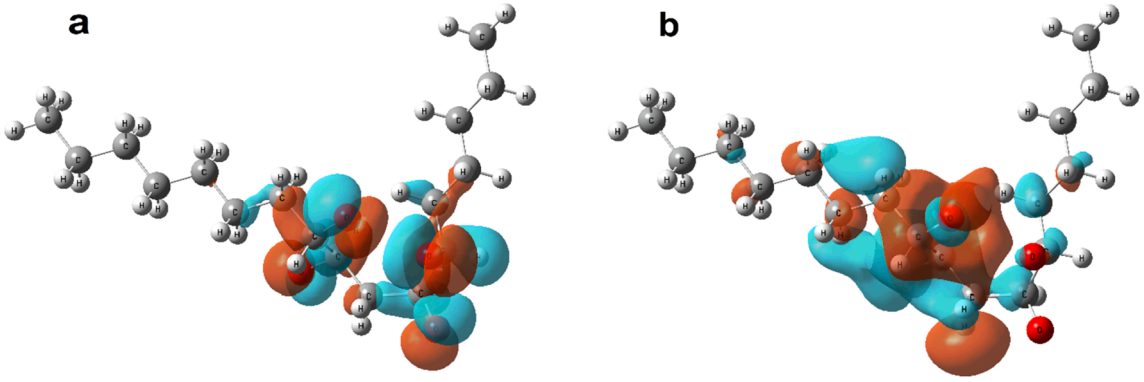

Fig. 6. HOMO (a) and LUMO (b) molecular orbitals of SFOL.

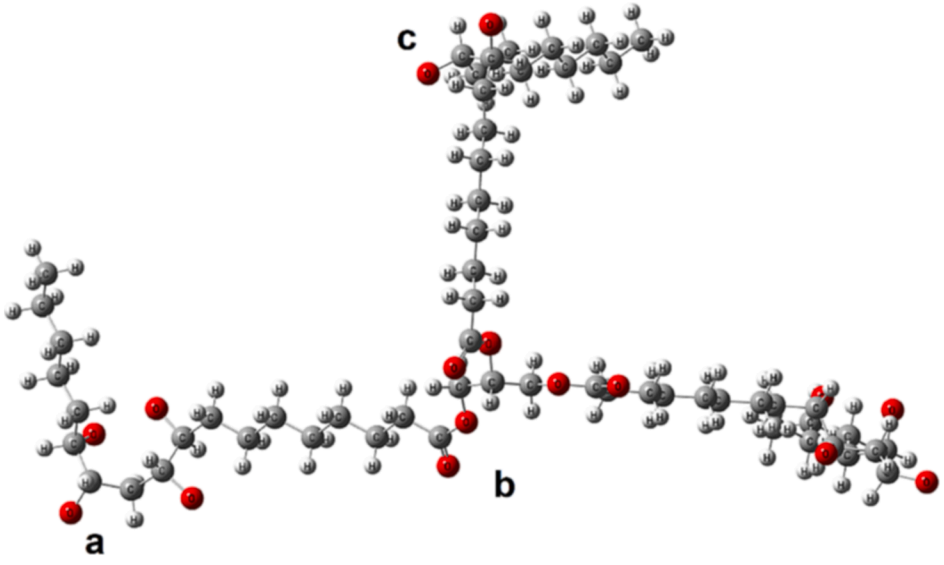

Fig. 7. MEP of SFOL and some points with most probability interaction with the metals.

common knowledge that TG/DSC is a reliable, less time consuming, and effective method for studying the heat effects and mass change variation throughout the process of HCO oxidation [66]. Moreover, the process of HCO oxidation is classified into two main regions: low temperature oxidation region (LTO) and high temperature oxidation region (HTO). During LTO region, the oxygen reacts with oil components to form oxygenated compounds such as hydrogen peroxides, alcohols, ketones, aldehydes, and other hydrocarbons. The LTO ends up usually with the formation of a solid condensed product known in the literature as fuel deposition or coke. During HTO, the oxidation of the obtained fuel

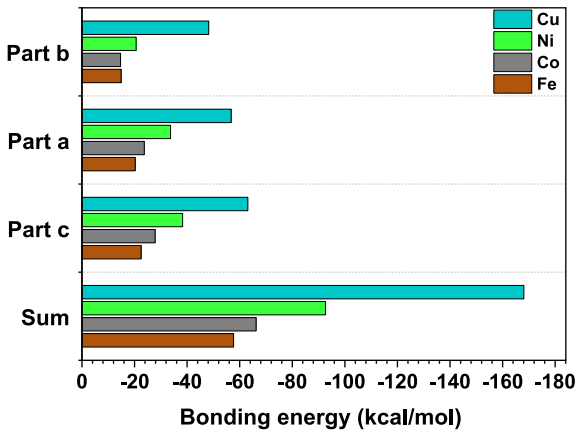

Fig. 8. Bonding energy (kcal/mol) between oxygen with the metals in different parts of SFOL.

Table 3
Bond strength (kcal/mol) of SFOL-metal at high temperatures.

Temperature (°C)	Fe	Co	Ni	Cu
25	−20.3	−23.7	−33.7	−56.8
250	−13.0	−14.2	−26.6	−46.5
350	−9.7	−11.2	−23.3	−21.2
450	−6.4	−9.3	−20.0	−16.3
$\Delta E_{(SFOL\text{-}metal)}$	13.9	14.4	13.7	40.5

deposit is occurred and leads to the formation of combustion front which is the main key for a successful in-situ combustion. Figs. 10 and 11 shows the DSC (a), TGA, and DTG curves (b) for oxidation of HCO without and with OSCs at different heating rates. The effect of the used OSCs was clearly showed by peak temperature shifting in both LTO and HTO oxidation. Interestingly, the effect of Cu-OSC was more significant compared with other metals whether in heat effect variation (DSC), where it was able to shift the HTO region by almost 120 °C from 500 °C in the absence of catalyst to almost 380 °C at 20 °C /min, or in terms of mass loss (TG/DTG) peaks where the peak shifted as well from 500 °C in the absence of catalyst to almost 380 °C at 20 °C/min. To the best of our knowledge, this is the first highly OSC that provided a highest temperature shift of 120 °C in HTO region compared with other reported OSCs in literature.

3.4. Analysis of OSCs transformation during and after HCO oxidation process

The transformations of OSCs in absence and presence of HCO under isothermal conditions at 350 °C and 500 °C for 4 h were carried out. The resulting solid products after the oxidation were analyzed by XRD and SEM. SEM images of solid products obtained after oxidation of OSCs in absence and presence of heavy oil at 350 °C and 500 °C are depicted in Fig. 12.

The morphologies of the products are different at 350 °C and 500 °C in presence or absence of HCO. For all samples, products with higher porosity were observed at 500 °C compared with 350 °C. At 350 °C, shape of Fe nanoparticles in Fe-OSC was changed from spherical to nano-tubes because of octahedral space group of Fe. In addition, temperature has a significant effect on the average of particle size. In all systems, the average of particle size at 500 °C was much lower than at 350 °C. For example, the average of particle size of Cu at 350 °C was in the range of 49–175 nm; however, its average size considerably decreased to the range of 19–82 nm at 500 °C. Co nanoparticles showed higher average of particle size of 53–113 nm and 47–185 nm at 350 °C and 500 °C, respectively (Fig. S3). These results point toward the idea that smaller Cu nanoparticles in Cu-OSC would generate an excellent performance on HCO oxidation kinetics and thermal behavior. XRD patterns of the products after the isothermal oxidation of OSCs with HCO are presented in Fig. 13.

A different set of reflections in XRD patterns of HCO + OSCs was observed after oxidation compared with those of pure OSCs (Fig. 3). Reflections of metal oxides appeared and the reflections of OSC phases almost were vanished at 500 °C. For Fe-OSC, Ni-OSC, Co-OSC, and Cu-OSC, XRD patterns of the residues correspond to α-Fe_2O_3 and γ-Fe_2O_3, NiO and Ni_2O_3, Co_3O_4, CuO, and Cu_2O, respectively. The obtained results from both SEM and XRD reveal that OSCs were decomposed into nano-sized metal oxides during oxidation, which preliminary leads us to expect a higher catalytic performance on the process of heavy oil oxidation in their presence.

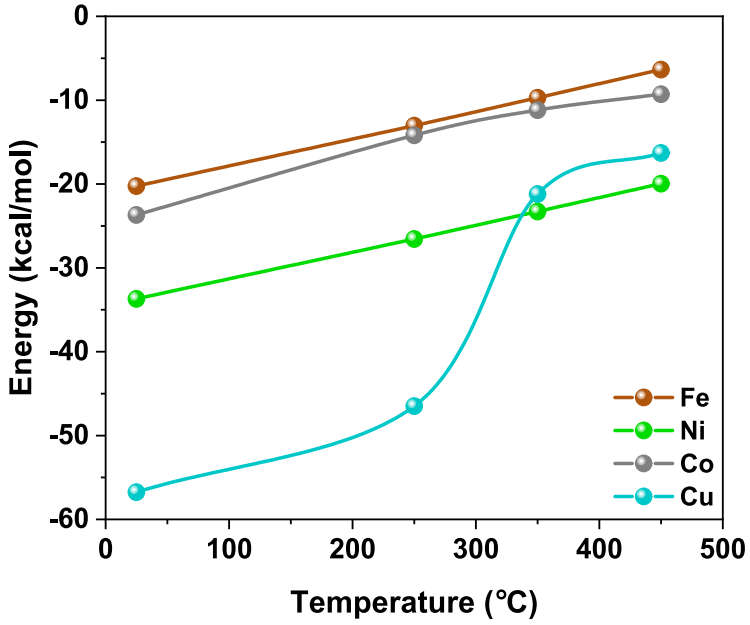

Fig. 9. Trend of bond energy changes with increasing temperature.

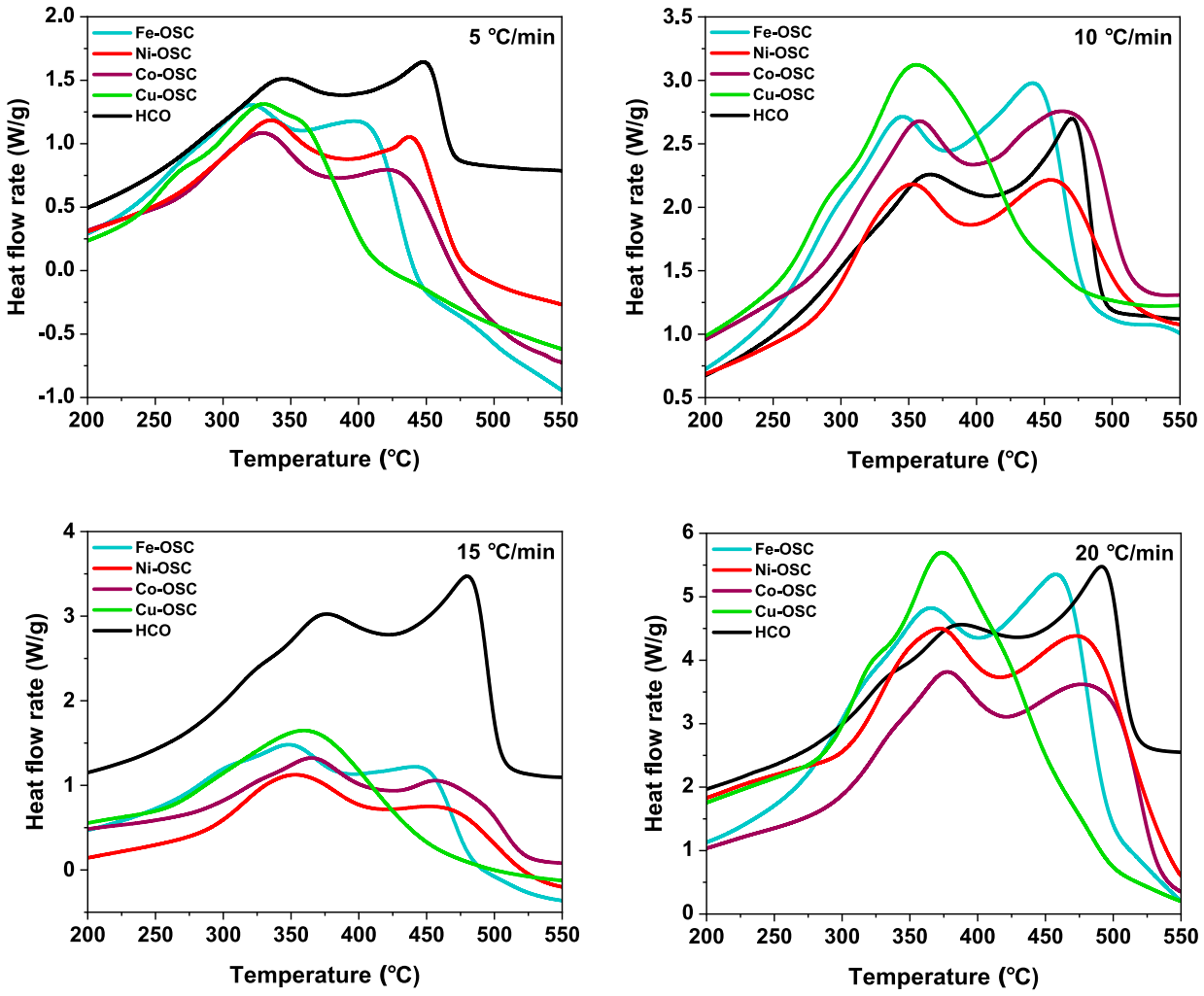

Fig. 10. DSC curves for oxidation of HCO in presence of OSCs at different heating rates.

3.5. Kinetic calculations

The results of TG, DTG and DSC curves are in good agreement with the computational results; however, additional evidence should be provided to support the hypothesis about the effect of ligand structure on HCO oxidation and effectiveness of the opted catalysts especially the Cu based one (Cu-OSC). For this reason, it is worthwhile to calculate kinetic and thermodynamic parameters of the process of HCO oxidation in presence and absence of OSCs.

It is common knowledge that heavy oil oxidation occurs in a complex multiphasic medium accompanied by different parallel and multistep reactions. This complicates the kinetic study of such processes comparing to kinetic calculations in homogeneous mediums. Therefore, the use of non-isothermal analysis facilitate the kinetic calculation of heavy oil oxidation based on the isoconversional principle which states that the kinetic parameters of solid phase thermal decomposition is a function of temperature only at constant conversion rate as expressed by the following equation [67]:

$$\frac{d\alpha}{dt} = k(T)P_{O_2}^{a}(1-\alpha)^{b} \quad (2)$$

where $k(T)$ is the reaction rate constant, expressed by Arrhenius law $k(T) = Ae^{-\frac{E}{RT}}(3)$, P_{O_2} is the oxygen partial pressure, and $(1-\alpha)^{b}$ is the reaction model function.

The oxygen partial pressure is generally considered constant during DSC experiments because of sample size (less than 1 mg in each run), the high of air flow rate (50 mL/min) and the large furnace volume (approx. 250 mL). Moreover, Fassihi et al. [68,69] have found out that the heavy oil oxidation reactions follow the first order $(b = 1)$ in the model function $f(\alpha) = (1-\alpha)^{b}$, which transforms equation (2) to:

$$\frac{d\alpha}{dt} = k_{eff}(1-\alpha) \quad (4),$$

where $k_{eff} = kP_{O_2}$

The activation energy and pre-exponential factor values dependencies on HCO conversion in our research were analyzed by using Friedman's [46] and Kissinger-Akahira-Sunose approaches based on the International Confederation for Thermal Analysis and Calorimetry (ICTAC) recommendations. It is worthy to note that these methods are considered among the first isoconversional methods proposed for non-isothermal kinetics treatment. The Friedman method is based on the following equation:

$$ln\left(\frac{d\alpha}{dt}\right)_{\alpha,i} = \ln[f(\alpha)A_{\alpha}] - \frac{E_{\alpha}}{RT_{\alpha,i}} \quad (5)$$

where i presents individual heating rate and $T_{\alpha,i}$ is the temperature at which conversion degree α is reached under the associated heating rate.

The Kissinger-Akahira-Sunose method is based on the equation (6):

$$ln\left(\frac{\beta_i}{T^2_{\alpha,i}}\right) = Const - \frac{E_{\alpha}}{RT_{\alpha,i}} \quad (6)$$

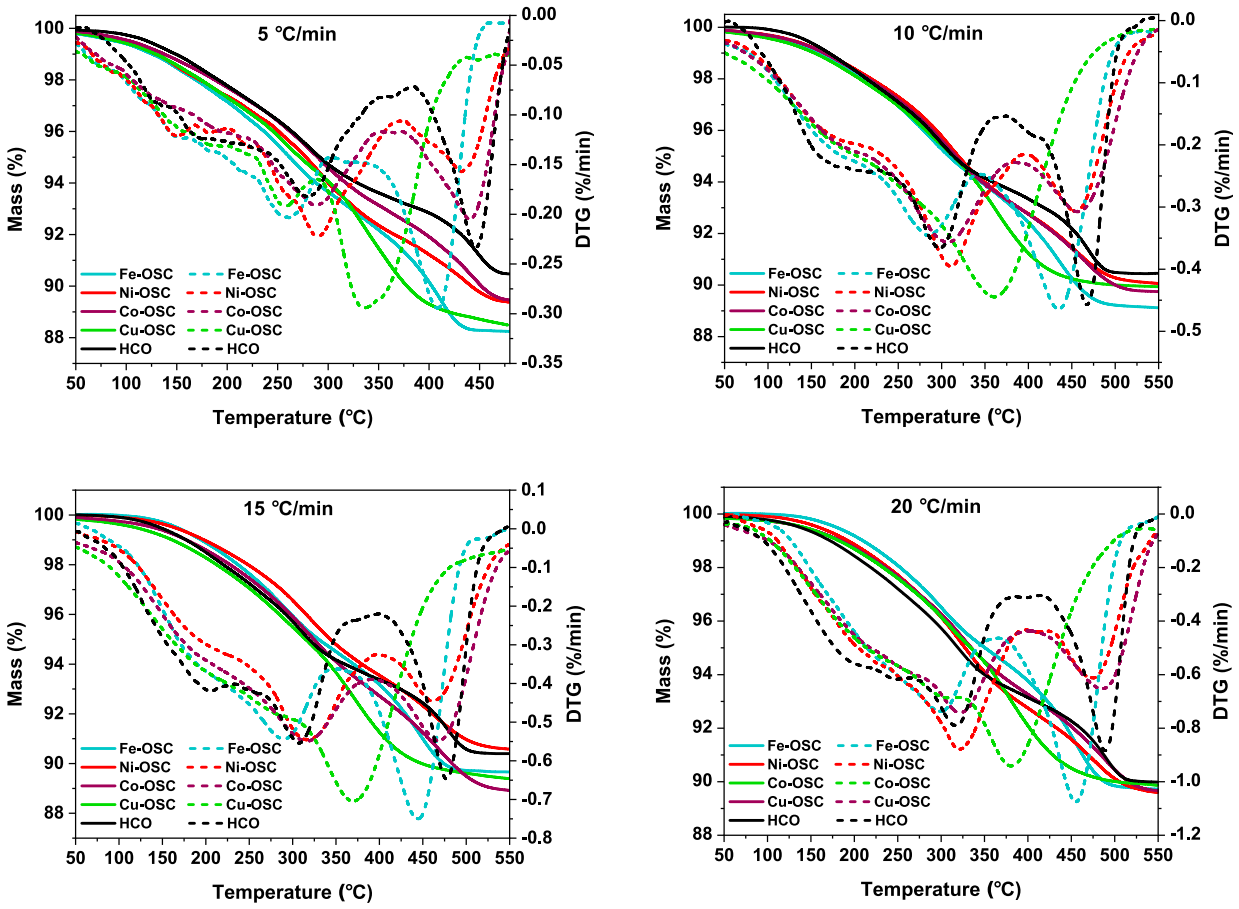

Fig. 11. TGA and DTG curves for oxidation of HCO in presence of OSCs at different heating rates.

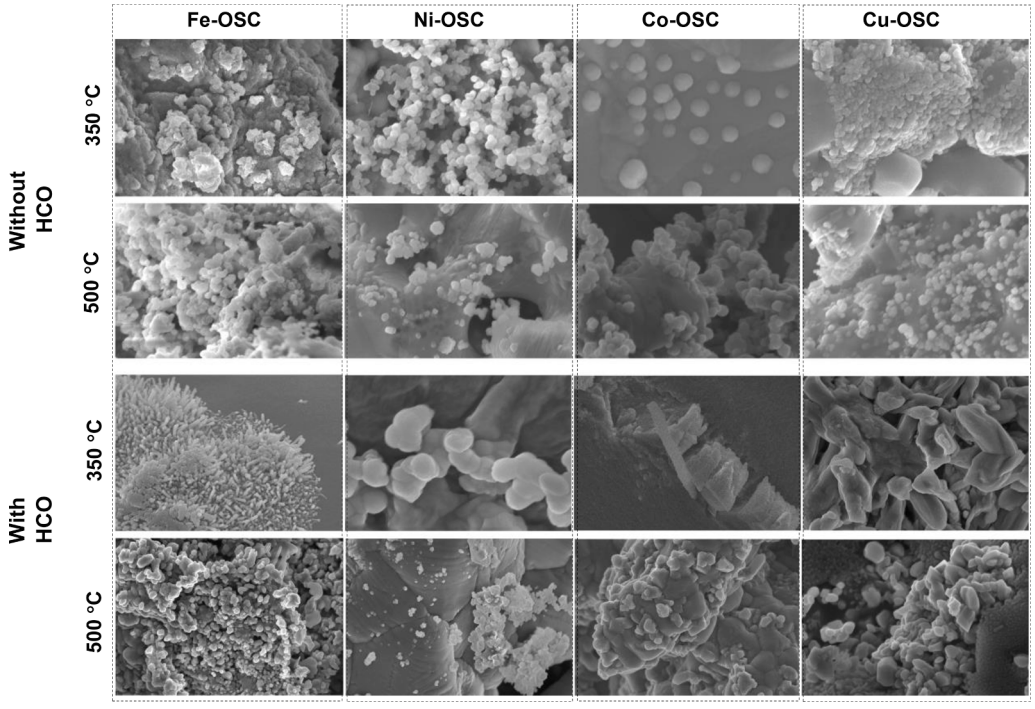

Fig. 12. SEM images of solid products obtained after oxidation of OSCs in absence and presence of HCO at 350 °C and 500 °C.

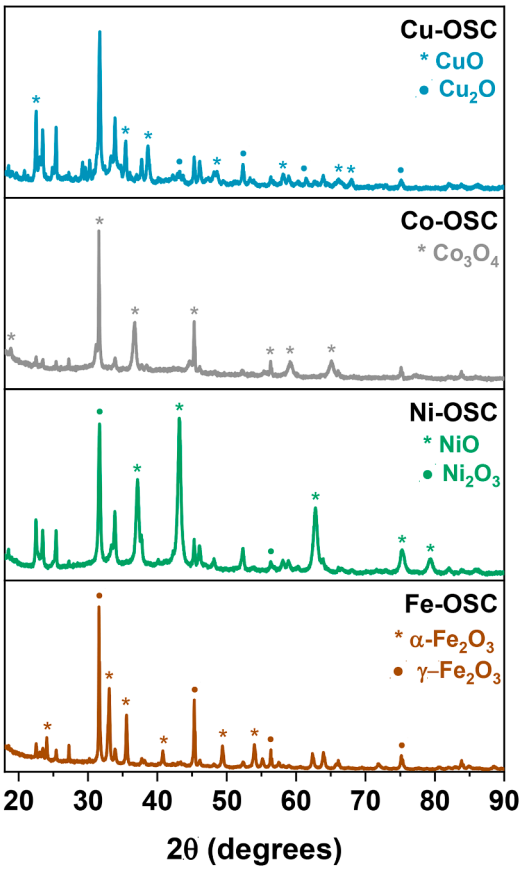

Fig. 13. XRD patterns of OSCs without and with HCO after oxidation at 500 °C.

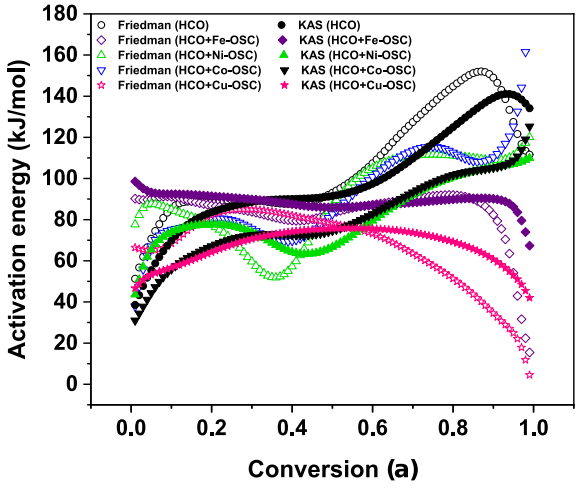

Fig. 14. Activation energy dependency on conversion of HCO oxidation process in presence and absence of OSCs obtained by Friedman and KAS methods.

The calculated values of activation energy and pre-exponential factor are presented in Fig. 14.

The evidence from Fig. 14 points toward the significant effect generated by the opted OSCs on HCO oxidation kinetic behavior for both KAS and Friedman analyses. In other words, all OSCs decreased the energies of activation of low and high temperature oxidation regions. The low temperature oxidation activation energy values in presence of OSCs were found to be less than those of the process of non-catalytic HCO oxidation. The lowest energy of activation of low temperature oxidation region was associated to Ni based catalyst Ni-OSC. At low temperature range, Ni metal species highlight a higher activity compared with other metals due to the formation of nickel oxide species (Figs. 12 and 13) which have a more tendency to oxygenated compounds such as hydrogen peroxide, carboxylic acids, aldehydes, and ketones (the main products of the first stage of HCO oxidation process) [70]. Moreover, the higher bonding energy between Ni and SFOL (Fig. 8 and Table 3) demonstrates thermal stability of Ni at this stage to exhibit its catalytic properties on HCO components in this zone. However, Cu-OSC provided the lowest energy of activation during the high temperature oxidation regions, which is the main region during the process of in-situ combustion as shown by Friedman and KAS analyses compared with other OSCs and pure HCO. Fe-based catalyst comes in the first place after Cu-OSC regarding activation energy decreasing followed by Ni-OSC and Co-OSC, from an efficiency point of view compared with the non-catalytic oxidation of HCO energy of activation. It is worthwhile noting that the higher metal dispersion in Cu-OSC (Fig. 4), the formation of the smallest particle size of copper oxide (Figs. 12 and 13) and the higher bonding energy with the SFOL at higher temperatures (Fig. 8) distinguish it among other OSCs where it allowed their higher contact with oil components during all the stages of HCO oxidation in both low and high temperature oxidation regions. Moreover, the higher thermal stability of SFOL guarantees a stable environment for metal transformation and oxidation in addition to creating the properties of anti-aggregating for the obtained copper oxide nanoparticles which results in small particle sizes. These nanoparticles possess a significant catalytic activity on high temperature oxidation region and stabilize the combustion front during in-situ combustion due to their high surface specific area. Moreover, Fig. 14 demonstrates two main regions as shown by two shoulders of the obtained curves, indicating the presence of LTO and HTO regions. Moreover, this exhibits the multistep trait of HCO oxidation in presence and absence of the used OSCs. However, no double shoulder behavior was observed in presence of Cu-based catalyst which signified contrarily-one shoulder instead of two. This again indicates the unique properties of Cu-OSC which is found to improve the hypotheses about the higher catalytic activity of Cu-based catalyst. To further support the obtained activation energy values by isoconversional approach, it is worthy to illustrate them by applying the model-based approach which predicts the kinetic behavior of HCO oxidation in presence and in the absence of OSCs (Fig. 15). A total of 36 two-step models were selected for the analysis by applying the F-test [71], which allowed optimal model selection and described the two-step reactions. Table 4 presents the kinetic parameters of HCO oxidation process obtained by the model approach of non-isothermal kinetics. A detailed consideration of each of the calculated models is presented in supplementary materials.

The resulting kinetic parameters indicate a similar tendency toward activation energy decreasing for the experiments with OSCs. Once again, the obtained results showed a significant impact of the opted catalysts on the process of HCO oxidation kinetic parameters. Additionally, Cu-OSC improved the process of HCO oxidation significantly where it allowed a considerable decrease in the value of activation energy. It was even less than the activation energy value of the LTO region of HCO oxidation in absence of catalysts or even for those experiments in presence of Ni-OSC and Co-OSC. The activation energy of HCO high temperature oxidation in presence of Cu-OSC was found to be 69.3 kJ/mole compared with LTO of non-catalytic oxidation, Fe-OSC, and Ni-OSC which were equal to 91.8, 81.9, and 85.3 kJ/mole, respectively. Given that our findings are based on activation energies dynamics, the kinetic study of such complicated processes in heterogenous media should therefore be treated by considering the whole equation of Arrhenius. In other words, unlike the positive effect generated by OSCs on the activation energy values of the HCO oxidation processes, the results seem to be contradictory in terms of their effect on the values of the preexponential factors of HCO high and low temperature oxidation regions. As can be seen from Table 4, OSCs have a negative effect on the values of the preexponential factors, which were expected to raise in

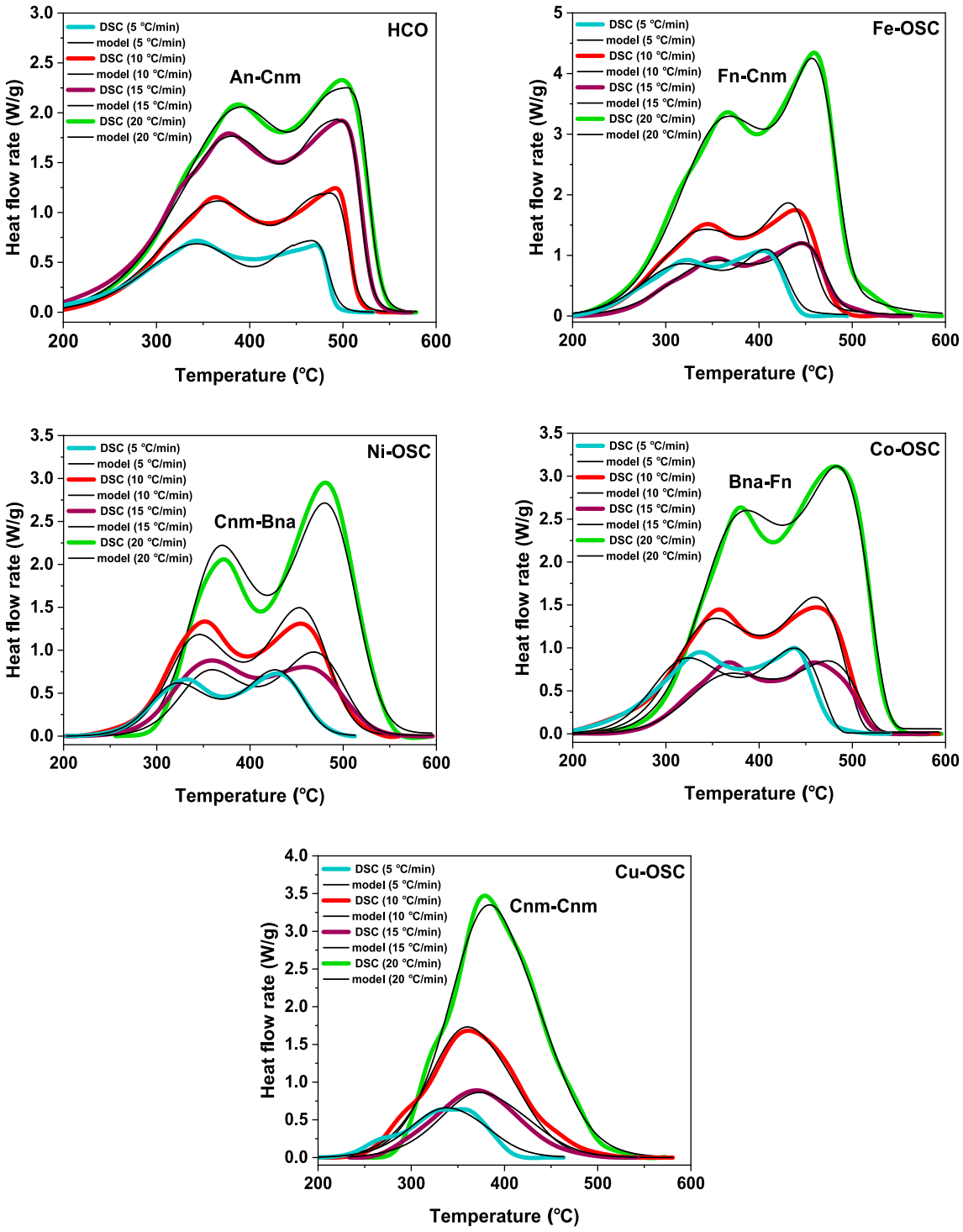

Fig. 15. DSC model fit curves for HCO oxidation in presence and absence of OSCs at different heating rates.

their presence as a complementary sign of significant impact on HCO oxidation reactions. Unfortunately, these results indicate that pre-exponential factor values decrease in presence of OSCs which leads to a reduction in the values of the reaction rates of the occurring reactions. It can be a negative factor for the function of OSCs. Thus, the total effect of the kinetic parameters on oxidation reaction rates should be estimated by calculating oil conversion time dependency on time at different conversion degrees based on the models obtained in Table 4 to confirm the positive effect of the catalysts.

3.6. Kinetic predictions

The role of OSCs in the processes of HCO oxidation from a kinetic point of view was further investigated by calculating the times corresponding to 10 %, 50 %, and 90 % of HCO oxidation based on the applied models. It is common knowledge that 10 % of HCO oxidation conversion is associated to LTO process as the beginning stages, meanwhile 50 % conversion is related to the LTO end stage and HTO starting stage, and 90 % conversion time is associated to the HTO peak [33]. The obtained HCO oxidation conversion times in OSC systems are presented

Table 4
Kinetic parameters of HCO oxidation process in presence and absence of OSCs obtained by the model approach of non-isothermal kinetics.

Kinetic parameters	Sample	LTO	HTO
E_a, kJ·mole^{-1}	HCO	91.8	149.1
	Fe-OSC	81.9	105.5
	Ni-OSC	85.3	102.9
	Co-OSC	66.5	119.7
	Cu-OSC	85.4	69.3
logA, A in s^{-1}	HCO	5.2	8.2
	Fe-OSC	4.6	5.3
	Ni-OSC	1.2	5.2
	Co-OSC	3.3	6.2
	Cu-OSC	3.3	2.7

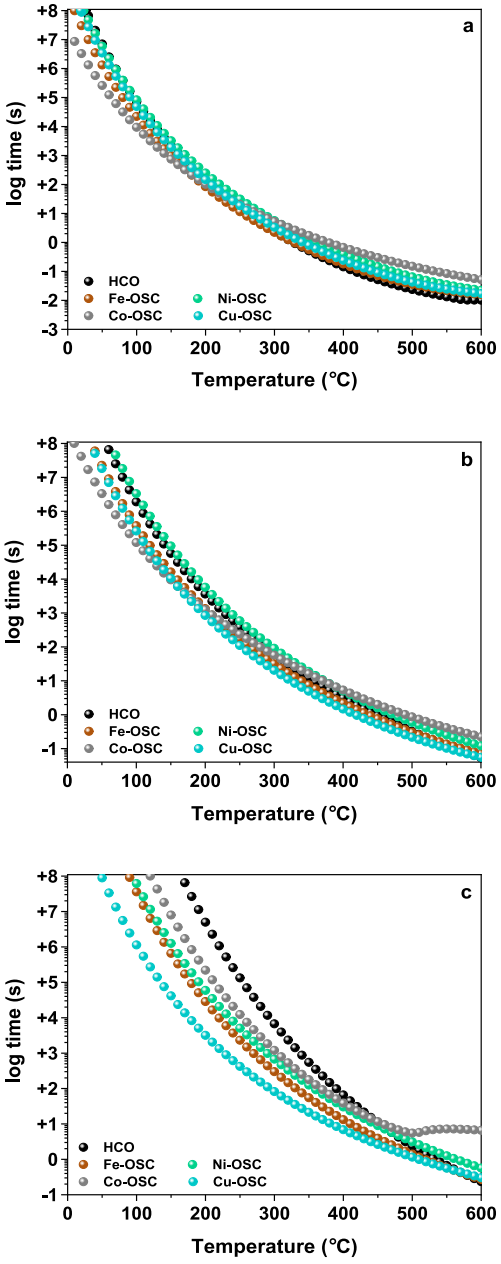

Fig. 16. Calculated oxidation times of HCO in presence and absence of OSCs at 10% (a), 50% (b), and 90% (c) of oxidation conversion.

in Fig. 16. The aim of calculating the oxidation times at different reaction conversions is to confirm the positive effect generated by OSCs at HTO, which is basically the most important stage in the application of in-situ combustion projects because it is responsible for promoting the combustion front propagation throughout the reservoir volume. All OSCs exhibited their higher catalytic activity at HTO as illustrated by the short conversion times especially at temperatures lower than 500 °C which is commonly known as the temperature of combustion end for HCO. Moreover, the obtained results are in good agreement with the previous hypotheses about the significant effect of Cu-OSC on the process of HCO oxidation where it showed the least oxidation conversion time that is associated to the highest reaction rate compared with the non-catalytic oxidation of HCO and other OSCs.

3.7. Thermodynamic study

Thermodynamic functions of the activated complexes formation during HCO oxidation in presence and absence of OSCs were studied to provide more insight into the effect of the catalysts. In general, reactants are found usually in equilibrium with activated complexes in chemical processes according to the transition state theory. Studying thermodynamic functions during the HCO oxidation improves the knowledge about the thermal dynamics and heat exchange processes. In fact, the thermodynamic functions characterize the equilibrium of decomposition process and can be calculated using the following equations:

$$\Delta^{\ddagger}H^0 = E_\alpha - RT_{st} \tag{7}$$

$$\Delta^{\ddagger}S^0 = R\left(ln\frac{hA_\alpha}{K_B T_{st}} - 1\right) \tag{8}$$

$$\Delta^{\ddagger}G^0 = \Delta^{\ddagger}H^0 - T_{st}\Delta^{\ddagger}S^0 \tag{9}$$

where K_B and h are the Boltzmann and Planck constants, respectively, $\Delta^{\ddagger}G^0$, $\Delta^{\ddagger}S^0$, and $\Delta^{\ddagger}H^0$ represents Gibbs's energy standard, entropy, and enthalpy of activated complex formation, respectively. T_{st} is an arbitrary chosen temperature which was defined as the first peak temperature at the minimum heating rate (613 K). The equations (7)-(9) require the knowledge of the activation energy and pre-exponential factor to calculate the thermodynamic functions of equilibrium. Friedman method was used to calculate these parameters as it requires minimum assumptions. The Gibbs energies, enthalpies and entropies calculated at different oxidation conversion are presented in Fig. 17 and Table S2.

As can be seen from Fig. 17, the thermodynamic functions that describe equilibrium between the reactants and activated complex depend strongly on the conversion. This indicates that oil oxidation is a complex process including various consecutive and parallel reactions. The change in the enthalpy ($\Delta^{\ddagger}H^0$) characterizes the amount of the energy required to reach the activated state. In all cases this change was found to be positive which indicates that the energy comes from the surrounding of the activated complex formation. Thus, if the required energy is high, the reaction rate is slow. Moreover, Fig. 17a highlights less values for HCO oxidation process enthalpy of activation in presence of OSCs at different conversions. This witnesses the positive effect of the catalysts especially in presence of Cu-OSC which exhibited the lowest enthalpy at higher conversion (HTO). Furthermore, the entropy $\Delta^{\ddagger}S^0$ change is known to be an accurate parameter for describing the disorder difference between oil components and the activated complex during HCO oxidation process. As shown in Fig. 17b, $\Delta^{\ddagger}S^0$values for the processes of the catalytic and non-catalytic oxidation are negative. This indicates that the activated complex is more ordered than the initial state in all systems. It should be noted that in presence of OSCs, the entropy of activation in most cases showed a more negative value compared with the non-catalytic oxidation of HCO. This indicates that more ordered complexes were formed in presence of the opted catalysts. The obtained entropy and enthalpy values confirm the results of

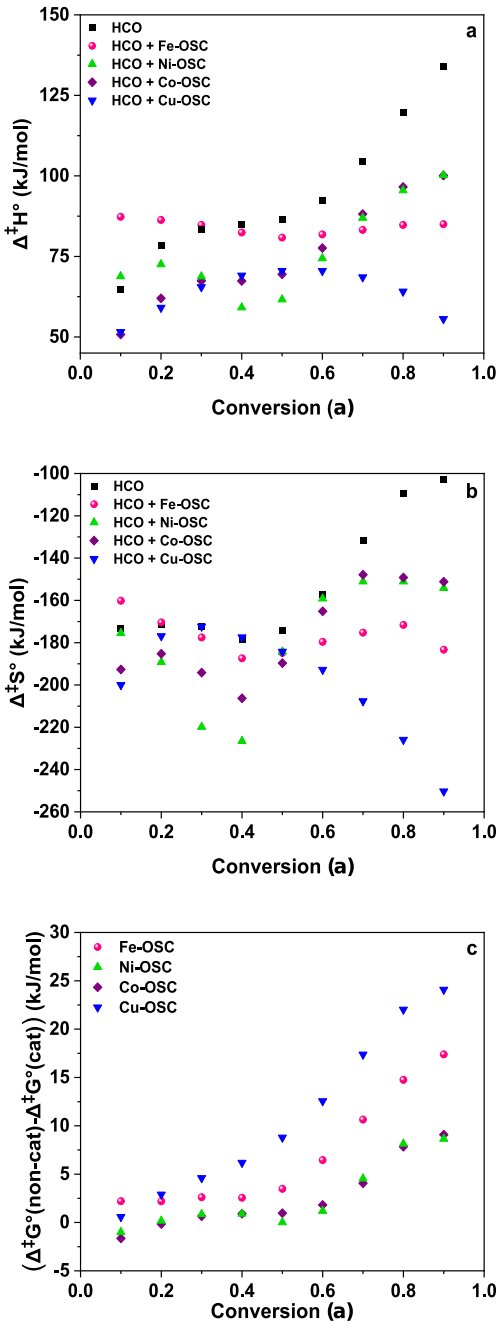

Fig. 17. Activation enthalpy dependency (a), activation entropy dependency (b) on conversion of the catalytic and non-catalytic HCO oxidation, and Gibbs's free energy of HCO oxidation in presence and absence of OSCs (c).

computational calculation (Fig. 8 and Table 3), which calculated the strength of bond energy between the SFOL and metals and found that Cu has the strongest bond energy with SFLO followed by Ni, Co and Fe. The values of the enthalpies related to these metals-based catalysts showed the same trend in terms of system order. In other words, the highest system order represents the strongest bond energy between the metal and SFOL as observed for Cu-OSC. Fig. 17b suggests the strongest energy bond between Cu and SFOL in presence of HCO at higher temperatures as shown by the lowest negative values of the system of HCO with Cu-OSC. In addition, the highest system order provided by Cu-OSC corroborates as well with the kinetic findings and the associated values of reaction rates obtained (Fig. 17). There is a satisfactory agreement between the SEM analysis, XRD patterns, and the computational investigation about the stability of the HCO-Cu-OSC system at higher temperatures which allowed the formation of non-aggregated nanoparticles of copper oxide at HTO and exhibit their catalytic activity on the process of HCO combustion without losing their electric and physical properties. This allows them to destruct and break down heavy components and coke product at this stage to improve heat generation, and therefore stabilize the combustion front. Fig. 17c presents the obtained results of Gibbs free energy of activation. In the literature, the Gibbs free energy of any process is usually used for expressing the amount of the activated complex being formed. More complex is formed in a system with lower Gibbs energy; therefore, the process will proceed faster. Thus, comparing Gibbs's free energy in the catalytic and non-catalytic oxidation of HCO demonstrate the efficiency of the OSCs and could provide more details on the individual roles of each metal interaction with the associated ligand and oil components. The values of Gibbs's free energy of HCO oxidation in presence and absence of OSCs are shown in Fig. 17c. The *y*-axis represents the difference between Gibbs's free energy ($\Delta^{\ddagger}G^{0}$(non-cat)) associated to HCO non-catalytic oxidation process and the Gibbs's free energy corresponding to HCO oxidation process in presence of OSCs ($\Delta^{\ddagger}G^{0}$(cat)).

According to Fig. 17c, it can be concluded that OSCs accelerate HCO oxidation rate significantly with conversion increment especially at HTO region. Moreover, Ni-OSC and Co-OSC have insignificant effect on the reaction rate at conversions below 0.5. However, the catalytic effect was significantly enhanced at higher conversions (HTO region), which gives up to 10 kJ mol^{-1} gain in the Gibbs energy. On another hand, Fe-OSC showed a similar trend as Ni-OSC and Co-OSC at lower conversion rates (less than 0.5) but with a linear increase in Gibbs energy at higher conversions rates (more than 0.5). It is worthy to note that Cu-OSC demonstrates the maximum catalytic activity where the Gibbs's free energies started at the beginning of the process and increased immediately in a linear manner. These observations reveal a significant effect of Cu-OSC especially on HTO and basically confirmed the results of the highest system order, the highest reaction oxidation, and the highest ligand–metal bonding energy, making it as a promising material for industrial application of in-situ-combustion for enhanced oil recovery.

4. Conclusions

This paper investigated the role of ligand structure and its interaction with different metals in oil soluble catalysts for enhancing heavy crude oil recovery by the in-situ combustion technique. Sunflower oil as a green and cheap source was used to synthesize a novel ligand for the preparation of effective oil soluble catalysts. The obtained results showed a strong bonding energy of the used metals with the ligand which provides a stable thermal property for the catalytic systems. The strongest bonding energy with ligand was found for Cu (40.5 kcal/mol) at different temperatures compared with Ni (13.7 kcal/mol), Co (14.4 kcal/mol), and Fe (13.9 kcal/mol). Moreover, the resulting metal oxides nanoparticles showed less sizes for copper oxide particles (49–175 nm), providing higher specific surface area during the high temperature oxidation region. The findings about the copper-based catalyst appeared to be well supported by non-isothermal kinetics and thermodynamic study which highlighted the impact of the obtained oil soluble catalysts with different metals on the process of HCO oxidation. As expected from computational results and formed metals oxides nanoparticles at high temperatures oxidation region, the synthesized catalysts exhibited excellent catalytic activity on decreasing the activation energy of high temperature oxidation from 149.1 KJ/mol in non-catalytic system to 105.5, 102.9, 119.7, and 69.3 KJ/mol in presence of Fe, Co, Ni, and Cu, respectively. These results were in a perfect agreement with the values of activation enthalpy, entropy and Gibbs's free energy of HCO high temperature oxidation at 0.7 conversion degree which were found to be equal to 122.3 KJ/mol, −131.9 J/mol, and 203.2 KJ/mol, respectively, for non-catalytic system compared with 85 KJ/mol, −175.3 J/mol, and 192.5 KJ/mol for Fe-OSC; 106.0 KJ/mol, −151.1 J/mol, and 198.6 KJ/

mol for Co-OSC; 108.4 KJ/mol, −147.9 J/mol, and 199.1 KJ/mol for Ni-OSC, and 58.5 KJ/mol, −207.7 J/mol and 185.8 KJ/mol for Cu-OSC. Even though all the synthesized catalysts generated a positive effect on HCO oxidation kinetics and thermodynamics functions, our findings suggest that the use of Cu-OSC could hypothetically lead to revolutionize the application of catalytic systems in the petroleum industry and would show a considerable effect on the worldwide economy which is directly related to the petroleum industry. These results clearly indicate that the structure of ligand has a predominant effect on efficiency of OSC and a stronger interaction of metal with ligand guarantees a highly effective catalytic system for HCO oxidation. We propose that further research should be undertaken in ramped temperature oxidation cells and combustion tubes at larger scales in presence of the obtained catalysts. It is expected that this research would be helpful in solving the combustion front propagation problem during the process of in-situ combustion and the obtained copper-based catalyst would be valuable in other enhanced oil recovery methods.

CRediT authorship contribution statement

Arash Tajik: Validation, Formal analysis, Investigation, Writing – original draft. **Abdolreza Farhadian:** Conceptualization, Project administration, Supervision, Validation, Resources, Visualization, Writing – original draft, Writing – review & editing. **Mohammed A. Khelkhal:** Supervision, Writing – original draft, Validation, Writing – review & editing. **Morteza Rezaeisadat:** Writing – original draft. **Sergey M. Petrov:** Resources, Validation. **Alexey A. Eskin:** Validation, Investigation, Formal analysis. **Alexey V. Vakhin:** Supervision, Resources, Validation. **Meisam Babapour Golafshani:** Validation, Investigation, Formal analysis. **Semen E. Lapuk:** Formal analysis, Investigation. **Alexey E. Buzurov:** Formal analysis, Investigation. **Airat Kiiamov:** Formal analysis, Investigation. **Jorge Ancheyta:** Supervision, Writing – review & editing, Validation.

Declaration of Competing Interest

The authors declare that they have no known competing financial interests or personal relationships that could have appeared to influence the work reported in this paper.

Data availability

Data will be made available on request.

Acknowledgment

This work was supported by the Russian Science Foundation (grant N°. 22-73-00329).

Appendix A. Supplementary data

Supplementary data to this article can be found online at https://doi.org/10.1016/j.cej.2022.139813.

References

[1] A.V. Vakhin, M.A. Khelkhal, A. Tajik, M.R. Gafurov, O.G. Morozov, A. R. Nasybullin, S.A. Karandashov, A.A. Ponomarev, T.O. Krapivnitskaia, M. Y. Glyavin, The Role of Nanodispersed Catalysts in Microwave Application during the Development of Unconventional Hydrocarbon Reserves: A Review of Potential Applications, Processes. 9 (2021) 420.
[2] I. Santos, P.F. Oliveira, C.R.E. Mansur, Factors that affect crude oil viscosity and techniques to reduce it: A review, Brazilian J. Pet. Gas. 11 (2017) 115–130.
[3] A.G.A. Jameel, A. Khateeb, A.M. Elbaz, A.-H. Emwas, W. Zhang, W.L. Roberts, S. M. Sarathy, Characterization of deasphalted heavy fuel oil using APPI (+) FT-ICR mass spectrometry and NMR spectroscopy, Fuel 253 (2019) 950–963.
[4] H. Li, H. Gao, X. Zhao, Z. Xia, B. Yu, D. Sun, Experimental study on viscosity reduction of heavy oil with water content by synergistic effect of microwave and nano-catalyst, J. Pet. Sci. Eng. 208 (2022), 109271.
[5] T. Babadagli, Philosophy of EOR, J. Pet. Sci. Eng. 188 (2020), 106930.
[6] C. Yuan, K. Sadikov, M. Varfolomeev, R. Khaliullin, W. Pu, A. Al-Muntaser, S. Saeed Mehrabi-Kalajahi, Low-temperature combustion behavior of crude oils in porous media under air flow condition for in-situ combustion (ISC) process, Fuel 259 (2020), 116293.
[7] S. Sitnov, I. Mukhamatdinov, F. Aliev, M.A. Khelkhal, O. Slavkina, K. Bugaev, Heavy oil aquathermolysis in the presence of rock-forming minerals and iron oxide (II, III) nanoparticles, Pet. Sci. Technol. 38 (2020) 574–579.
[8] A.S. Ushakova, V. Zatsepin, M.A. Khelkhal, S.A. Sitnov, A.V. Vakhin, In Situ Combustion of Heavy, Medium, and Light Crude Oils: Low-Temperature Oxidation in Terms of a Chain Reaction Approach, Energy Fuels 36 (2022) 7710–7721.
[9] F.A. Aliev, I.I. Mukhamatdinov, S.A. Sitnov, M.R. Ziganshina, Y.V. Onishchenko, A. V. Sharifullin, A.V. Vakhin, In-situ heavy oil aquathermolysis in the presence of nanodispersed catalysts based on transition metals, Processes. 9 (2021) 127.
[10] C. Yuan, D.A. Emelianov, M.A. Varfolomeev, Oxidation Behavior and Kinetics of Light, Medium, and Heavy Crude Oils Characterized by Thermogravimetry Coupled with Fourier Transform Infrared Spectroscopy, Energy Fuels 32 (2018) 5571–5580.
[11] A.M. Elbaz, W.L. Roberts, PM from the combustion of heavy fuel oils, Energy. 152 (2018) 455–465.
[12] A.G.A. Jameel, Y. Han, O. Brignoli, S. Telalović, A.M. Elbaz, H.G. Im, W.L. Roberts, S.M. Sarathy, Heavy fuel oil pyrolysis and combustion: Kinetics and evolved gases investigated by TGA-FTIR, J. Anal. Appl. Pyrolysis. 127 (2017) 183–195.
[13] C. Yuan, N. Rodionov, S. Mehrabi-Kalajahi, D.A. Emelianov, A.L. Zinnatullin, M. A. Varfolomeev, R. Zairov, A. Stepanov, A.R. Mustafina, A. Al-Muntaser, Catalytic combustion of heavy oil using γ-Fe2O3 nanocatalyst in in-situ combustion process, J. Pet. Sci. Eng. 209 (2022), 109819.
[14] A.M. Elbaz, A. Gani, N. Hourani, A.-H. Emwas, S.M. Sarathy, W.L. Roberts, TG/DTG, FT-ICR mass spectrometry, and NMR spectroscopy study of heavy fuel oil, Energy Fuels 29 (2015) 7825–7835.
[15] Y. Li, Z. Wang, Z. Hu, B. Xu, Y. Li, W. Pu, J. Zhao, A review of in situ upgrading technology for heavy crude oil, Petroleum. 7 (2020) 117–122.
[16] C. Yuan, D.A. Emelianov, M.A. Varfolomeev, M. Abaas, Comparison of oxidation behavior of linear and branched alkanes, Fuel Process. Technol. 188 (2019) 203–211.
[17] C. Yuan, D.A. Emelianov, M.A. Varfolomeev, N.O. Rodionov, M.A. Suwaid, I. R. Vakhitov, Mechanistic and kinetic insight into catalytic oxidation process of heavy oil in in-situ combustion process using copper (II) stearate as oil soluble catalyst, Fuel 284 (2021), 118981.
[18] K.A. Ariskina, C. Yuan, M. Abaas, D.A. Emelianov, N. Rodionov, M.A. Varfolomeev, Catalytic effect of clay rocks as natural catalysts on the combustion of heavy oil, Appl. Clay Sci. 193 (2020), 105662.
[19] H. Berna, C.M. Ross, L.M. Castanier, A.R. Kovscek, Fuel formation and conversion during in-situ combustion of crude oil, SPE J. 18 (2013) 1217–1228.
[20] M.A. Varfolomeev, C. Yuan, A.V. Bolotov, I.F. Minkhanov, S. Mehrabi-Kalajahi, E. R. Saifullin, M.M. Marvanov, E.R. Baygildin, R.M. Sabiryanov, A. Rojas, Effect of copper stearate as catalysts on the performance of in-situ combustion process for heavy oil recovery and upgrading, J. Pet. Sci. Eng. 207 (2021), 109125.
[21] Y. Chen, H. Yin, D. He, H. Gong, Z. Liu, Y. Liu, X. Zhang, W. Pu, Low temperature oxidized coke of the ultra-heavy oil during in-situ combustion process: Structural characterization and evolution elucidation, Fuel 313 (2022), 122676.
[22] A. Hart, M. Greaves, J. Wood, A comparative study of fixed-bed and dispersed catalytic upgrading of heavy crude oil using-CAPRI, Chem. Eng. J. 282 (2015) 213–223.
[23] S.L. Wellington, M.L. Joshi, J. Cui, S.N. Milam, M.A. Reynolds, Method for treating a hydrocarbon containing formation US7841407B2 (2010).
[24] U.U. Amanam, A.R. Kovscek, Analysis of the effects of copper nanoparticles on in-situ combustion of extra heavy-crude oil, J. Pet. Sci. Eng. 152 (2017) 406–415.
[25] C. Yuan, M.A. Varfolomeev, D.A. Emelianov, M.A. Suwaid, A.A. Khachatrian, V. L. Starshinova, I.R. Vakhitov, A.A. Al-Muntaser, Copper stearate as a catalyst for improving the oxidation performance of heavy oil in in-situ combustion process, Appl. Catal. A Gen. 564 (2018) 79–89.
[26] A. Simão, E. Domínguez-Álvarez, C. Yuan, M.A. Suwaid, M.A. Varfolomeev, J. Ancheyta, O.F. Al-mishaal, S.I. Kudryashov, I.S. Afanasiev, D.A. Antonenko, On the use of metallic nanoparticulated catalysts for in-situ oil upgrading, Fuel 313 (2022), 122677.
[27] C. Li, W. Huang, C. Zhou, Y. Chen, Advances on the transition-metal based catalysts for aquathermolysis upgrading of heavy crude oil, Fuel 257 (2019), 115779.
[28] M. Babapour Golafshani, M.A. Varfolomeev, S. Mehrabi-Kalajahi, N.O. Rodionov, P. Tahay, A.L. Zinnatullin, D.A. Emelianov, F.G. Vagizov, K.G. Sadikov, Y.N. Osin, Oxidation of Heavy Oil Using Oil-Dispersed Transition Metal Acetylacetonate Catalysts for Enhanced Oil Recovery, Energy Fuels 35 (2021) 20284–20299.
[29] M.A. Khelkhal, A.A. Eskin, S.A. Sitnov, A.V. Vakhin, Impact of Iron Tallate on the Kinetic Behavior of the Oxidation Process of Heavy Oils, Energy Fuels 33 (2019) 7678–7683.
[30] T.A. Al-Attas, S.A. Ali, M.H. Zahir, Q. Xiong, S.A. Al-Bogami, Z.O. Malaibari, S. A. Razzak, M.M. Hossain, Recent advances in heavy oil upgrading using dispersed catalysts, Energy Fuels 33 (2019) 7917–7949.
[31] M.A. Khelkhal, A.A. Eskin, D.K. Nurgaliev, A.V. Vakhin, Thermal Study on Stabilizing the Combustion Front via Bimetallic Mn@Cu Tallates during Heavy Oil Oxidation, Energy Fuels 34 (2020) 5121–5127.
[32] E.R. Saifullin, S. Mehrabi-Kalajahi, C. Yuan, M.A. Varfolomeev, N.O. Rodionov, S. Talipov, K.G. Sadikov, Catalytic combustion of heavy crude oil by oil-dispersed copper-based catalysts: Effect of different organic ligands, Fuel 316 (2022), 123335.

[33] A. Farhadian, M.A. Khelkhal, A. Tajik, S.E. Lapuk, M. Rezaeisadat, A.A. Eskin, N. O. Rodionov, A.V. Vakhin, Effect of Ligand Structure on the Kinetics of Heavy Oil Oxidation: Toward Biobased Oil-Soluble Catalytic Systems for Enhanced Oil Recovery, Ind. Eng. Chem. Res. 60 (2021) 14713–14727.
[34] M.A. Khelkhal, A.A. Eskin, A.V. Vakhin, Kinetic Study on Heavy Oil Oxidation by Copper Tallates, Energy Fuels 33 (2019) 12690–12695.
[35] N.N. Petrukhina, G.P. Kayukova, G.V. Romanov, B.P. Tumanyan, L.E. Foss, I. P. Kosachev, R.Z. Musin, A.I. Ramazanova, A.V. Vakhin, Conversion processes for high-viscosity heavy crude oil in catalytic and noncatalytic aquathermolysis, Chem. Technol. Fuels Oils. 50 (2014) 315–326.
[36] F. Zhao, Y. Liu, Z. Fu, X. Zhao, Using hydrogen donor with oil-soluble catalysts for upgrading heavy oil, Russ. J. Appl. Chem. 87 (2014) 1498–1506.
[37] A. Yusuf, R.S. Al-Hajri, Y.M. Al-Waheibi, B.Y. Jibril, In-situ upgrading of Omani heavy oil with catalyst and hydrogen donor, J. Anal. Appl. Pyrolysis. 121 (2016) 102–112.
[38] W.L. Qin, Z.L. Xiao, The researches on upgrading of heavy crude oil by catalytic aquathermolysis treatment using a new oil-soluble catalyst, in: Adv. Mater. Res., Trans Tech Publ, 2013: pp. 1428–1432.
[39] M.A. Suwaid, M.A. Varfolomeev, A.A. Al-Muntaser, N.I. Abdaljalil, R. Djimasbe, N. O. Rodionov, A. Zinnatullin, F.G. Vagizov, Using the oil-soluble copper-based catalysts with different organic ligands for in-situ catalytic upgrading of heavy oil, Fuel 312 (2022), 122914.
[40] M.A. Khelkhal, A.A. Eskin, I.I. Mukhamatdinov, D.A. Feoktistov, A.V. Vakhin, Comparative Kinetic Study on Heavy Oil Oxidation in the Presence of Nickel Tallate and Cobalt Tallate, Energy Fuels 33 (2019) 9107–9113.
[41] A. Farhadian, M.A. Varfolomeev, M. Rezaeisadat, A.P. Semenov, A.S. Stoporev, Toward a bio-based hybrid inhibition of gas hydrate and corrosion for flow assurance, Energy. 210 (2020), 118549.
[42] A. Farhadian, A. Rahimi, N. Safaei, A. Shaabani, E. Sadeh, M. Abdouss, A. Alavi, Exploration of Sunflower Oil As a Renewable Biomass Source to Develop Scalable and Highly Effective Corrosion Inhibitors in a 15% HCl Medium at High Temperatures, ACS Appl. Mater. Interfaces. 13 (2021) 3119–3138.
[43] A. Farhadian, A. Heydari, M. Maddah, M.S. Hosseini, E. Sadeh, K. Peyvandi, F. Varaminian, Renewable biosurfactants for energy-efficient storage of methane: An experimental and computational investigation, Chem. Eng. J. 427 (2021), 131723.
[44] S. Vyazovkin, A.K. Burnham, J.M. Criado, L.A. Pérez-Maqueda, C. Popescu, N. Sbirrazzuoli, ICTAC Kinetics Committee recommendations for performing kinetic computations on thermal analysis data, Thermochim. Acta. 520 (2011) 1–19.
[45] S.E. Lapuk, L.S. Zubaidullina, M.A. Ziganshin, T.A. Mukhametzyanov, C. Schick, A. V. Gerasimov, Kinetic stability of amorphous solid dispersions with high content of the drug: A fast scanning calorimetry investigation, Int. J. Pharm. 562 (2019) 113–123.
[46] H.L. Friedman, Kinetics of thermal degradation of char-forming plastics from thermogravimetry. Application to a phenolic plastic, in: J. Polym. Sci. Part C Polym. Symp., Wiley Online Library, 1964: pp. 183–195.
[47] S. Vyazovkin, Some basics en route to isoconversional methodology, in: Isoconversional Kinet. Therm. Stimul. Process., Springer, 2015: pp. 1–25.
[48] S. Vyazovkin, A.K. Burnham, L. Favergeon, N. Koga, E. Moukhina, L.A. Pérez-Maqueda, N. Sbirrazzuoli, ICTAC Kinetics Committee recommendations for analysis of multi-step kinetics, Thermochim. Acta. 689 (2020), 178597.
[49] S. Vyazovkin, Isoconversional kinetics of thermally stimulated processes, Springer, 2015.
[50] S.E. Lapuk, T.A. Mukhametzyanov, C. Schick, A.V. Gerasimov, Crystallization kinetics and glass-forming ability of rapidly crystallizing drugs studied by Fast Scanning Calorimetry, Int. J. Pharm. 599 (2021), 120427.
[51] S.E. Lapuk, T.A. Mukhametzyanov, C. Schick, A.V. Gerasimov, Kinetic stability of amorphous dipyridamole: A fast scanning calorimetry investigation, Int. J. Pharm. 574 (2020), 118890.
[52] F. Jensen, Introduction to computational chemistry, John wiley & sons, 2017.
[53] C.Y. David, Computational chemistry, John wiley & sons, 2001.
[54] R. Dennington, T.A. Keith, J. M. Millam, GaussView, Version 6, Semichem Inc 2016.
[55] M.J. Frisch, G.W. Trucks, H.B. Schlegel, G.E. Scuseria, M.A. Robb, J.R. Cheeseman, G. Scalmani, V. Barone, B. Mennucci, G.A. Petersson, H. Nakatsuji, M. Caricato, X. Li, H.P. Hratchian, A.F. Izmaylov, J. Bloino, G. Zheng, J.L. Sonnenberg, M. Hada, M. Ehara, K. Toyota, R. Fukuda, J. Hasegawa, M. Ishida, T. Nakajima, 2009. Gaussian09. Gaussian Inc. 2009.
[56] T. Yanai, D.P. Tew, N.C. Handy, A new hybrid exchange–correlation functional using the Coulomb-attenuating method (CAM-B3LYP), Chem. Phys. Lett. 393 (2004) 51–57.
[57] T.H. Dunning Jr, Gaussian basis sets for use in correlated molecular calculations. I. The atoms boron through neon and hydrogen, J. Chem. Phys. 90 (1989) 1007–1023.
[58] T. Mineva, N. Russo, Solvent effects computed with the Gaussian density functional method, Int. J. Quantum Chem. 61 (1997) 665–671.
[59] J.W. Ochterski, Thermochemistry in gaussian, Gaussian Inc. 1 (2000) 1–19.
[60] A. Heidarshenas, Z. Azizi, S.M. Peyghambarzadeh, S. Sayyahi, Experimental investigation of the particle size effect on heat transfer coefficient of Al 2 O 3 nanofluid in a cylindrical microchannel heat sink, J. Therm. Anal. Calorim. 141 (2019) 1–11.
[61] T. Schlick, Molecular modeling and simulation: an interdisciplinary guide, Springer Science & Business Media, 2010.
[62] J.H. Jensen, Molecular modeling basics, CRC Press, 2010.
[63] F. Weinhold, C.R. Landis, Natural bond orbitals and extensions of localized bonding concepts, Chem. Educ. Res. Pract. 2 (2001) 91–104.
[64] J.-O. Joswig, S. Roy, P. Sarkar, M. Springborg, Stability and bandgap of semiconductor clusters, Chem. Phys. Lett. 365 (2002) 75–81.
[65] J.S. Murray, P. Politzer, The electrostatic potential: an overview, Wiley Interdiscip. Rev. Comput. Mol. Sci. 1 (2011) 153–163.
[66] M.A. Khelkhal, S.E. Lapuk, A.V. Buzyurov, N.E. Ignashev, E.I. Shmeleva, I. I. Mukhamatdinov, A.V. Vakhin, Thermal Behavior of Heavy Oil Catalytic Pyrolysis and Aquathermolysis, Catalysts. 12 (2022) 449.
[67] P.S. Sarathi, In-situ combustion handbook–principles and practices, National Petroleum Technology Office, Tulsa, OK (US), 1999.
[68] M.R. Fassihi, W.E. Brigham, H.J. Ramey Jr, Reaction Kinetics of In-Situ Combustion: Part 2–Modeling, Soc. Pet. Eng. J. 24 (1984) 408–416.
[69] I.S. Bousaid, H.J. Ramey, Oxidation of Crude Oil in Porous Media, Soc. Pet. Eng. J. 8 (1968) 137–148.
[70] I.A. Sizova, A.B. Kulikov, M.I. Onishchenko, S.I. Serdyukov, A.L. Maksimov, Synthesis of nickel-tungsten sulfide hydrodearomatization catalysts by the decomposition of oil-soluble precursors, Pet. Chem. 56 (2016) 44–50.
[71] J.E. Freund, B.M. Perles, Modern elementary statistics, Pearson College Division, 2007.